Journal of Advanced Research 29 (2021) 137–145

Contents lists available at ScienceDirect

Journal of Advanced Research

journal homepage: www.elsevier.com/locate/jare

Programmable constant phase element realization with crossbar arrays

M.E. Fouda [a,b,*], A.M. AbdelAty [c], A.S. Elwakil [d,e,f], A.G. Radwan [a,f], A.M. Eltawil [b,g]

[a] Engineering Mathematics and Physics Dept., Faculty of Engineering, Cairo University, Egypt
[b] Electrical Engineering and Computer Science Dept., University of California-Irvine, Irvine, USA
[c] Engineering Mathematics and Physics Dept., Faculty of Engineering, Fayoum University, Egypt
[d] Department of Electrical and Computer Engineering, University of Sharjah, Sharjah, United Arab Emirates
[e] Department of Electrical and Computer Engineering, University of Calgary, Canada
[f] School of Engineering and Applied Sciences, Nile University, Giza, Egypt
[g] King Abdullah Univ. of Science and Technology, Thuwal 23955, Saudi Arabia

GRAPHICAL ABSTRACT

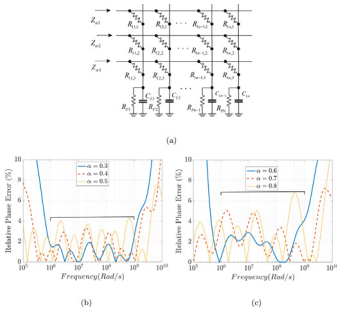

ARTICLE INFO

Article history:
Received 13 April 2020
Revised 5 August 2020
Accepted 11 August 2020
Available online 26 August 2020

Keywords:
Memristor
Crossbar array
CPE
Fractional-order capacitor
Approximation
Flower pollination algorithm

ABSTRACT

Introduction: Constant Phase Elements (CPEs) have been widely used in many applications due to the extra degree of freedom, which offers new responses and behaviors.
Objectives: This paper proposes a new programmable CPE realization using resistive crossbar arrays. By programming the resistive devices, different CPEs can be obtained.
Methods: The proposed realization can be approximated as a weighted sum of low and high pass filters having the same cut-off frequency (i.e., Lapicque model). The closed-form approximation expression is derived, and then the Flower Pollination Algorithm (FPA) is used to find the optimal values of the network components.
Results: Different design examples are given over the frequency range of $10^{6\text{-}10^9}$ rad/sec to prove the ability of this realization achieving any fractional order with less than 5% relative error in both phase and pseudo-capacitance. Monte-Carlo simulations are performed to evaluate the sensitivity of the proposed realization against device variability. In addition, multiple CPEs can be designed at the same time by utilizing the multiple ports of the crossbar array. The proposed realization is compared with two other state-of-art realizations showing comparable results as standalone realization and within fractional-order relaxation oscillator application.
Conclusion: The proposed crossbar realization has proven its ability to realize any CPE with acceptable error. In addition, this multiple-port design offers high flexibility and on-the-fly switching of the CPE.

Peer review under responsibility of Cairo University.
* Corresponding author.
E-mail address: foudam@uci.edu (M.E. Fouda).

https://doi.org/10.1016/j.jare.2020.08.007
2090-1232/

Introduction

Recently, programmable crossbar architectures have been used in many applications [1]. A crossbar array is constructed from interconnect metal wires, which are positioned in a cross-point shape. In each cross-point, a switch device is sandwiched between the metal wires, as shown in Fig. 2(a). The crossbar arrays have a small area footprint and can be stacked, creating 3D structures [2,3]. The recent progress in emerging memory technologies (such as RRAM or STT-RAM or PCM) that can be programmed to any analog value, enables performing many analog and digital applications with such a simple structure [4]. Crossbar arrays offer high flexibility for many applications due to their programmability and non-volatility such as in-memory computing, cryptography and physical unclonable functions (PUFs) [1,5,6]. Most recently, crossbar arrays have been used to accelerate neural networks training where the crossbar array does the vector-matrix multiplication naturally in one step, unlike digital implementations which require n^2 steps at least (n is the vector dimension). RRAMs are promising candidates in crossbar arrays since they have higher analog precision, low access and write times as well as high retention and endurance [5,4].

In our previous work [7], a closed-form modeling of the crossbar arrays (accounting for the loading and the parasitic effects) was derived. Interestingly, the network was modeled as a system of first-order differential equations, which can be used in many applications. This inspires us to investigate using crossbar arrays in new applications such as the here within proposed programmable realization of constant phase elements (CPEs) (known also as fractional-order capacitors).

CPEs are crucial devices in all applications of fractional-order system, such as oscillators, filters, and signal processing [8,9] although they are still not available off-the-shelf. To approximate fractional-order operators, infinite, semi-infinite, and finite-dimensional, integer-order systems are usually used in order to facilitate testing until reliable fractional-order elements become available [10].

The admittance of a CPE is given by:

$$Y(s) = C_\alpha s^\alpha, \tag{1}$$

where C_α is the pseudo-capacitance having units of $F \cdot \sec^{\alpha-1}$, and α, $0 < \alpha < 1$, is the fractional order. Practically, the constant phase behavior is observed in a certain frequency band known as the constant phase zone. So, an element with constant phase over all frequencies is a theoretical abstraction that cannot be obtained or approximated. These narrow-band frequency realizations are termed pseudo-fractional order elements (P-FOEs) [11]. Fig. 1 depicts a mind map for the state-of-art realizations and approximation methods of CPEs. It is noted that two-terminal device realizations are based on electrochemical material properties [9] such as ionic gel-Cu electrodes, graphene-polymer dielectrics or metal-polymer composites among others [12–16].

An approximating transfer function is often needed for analog multi-component realizations of CPEs in order to calculate the component values based on a selected network (e.g. Foster or Cauer network). Different methods are available to obtain these approximating transfer functions [17–19]. These transfer functions can be synthesized using passive or active circuits. The main advantage of active emulation is the electronic tunability of the fractional order and/or pseudo-capacitance values [20]. However, passive realizations remain to be the simplest and most widely

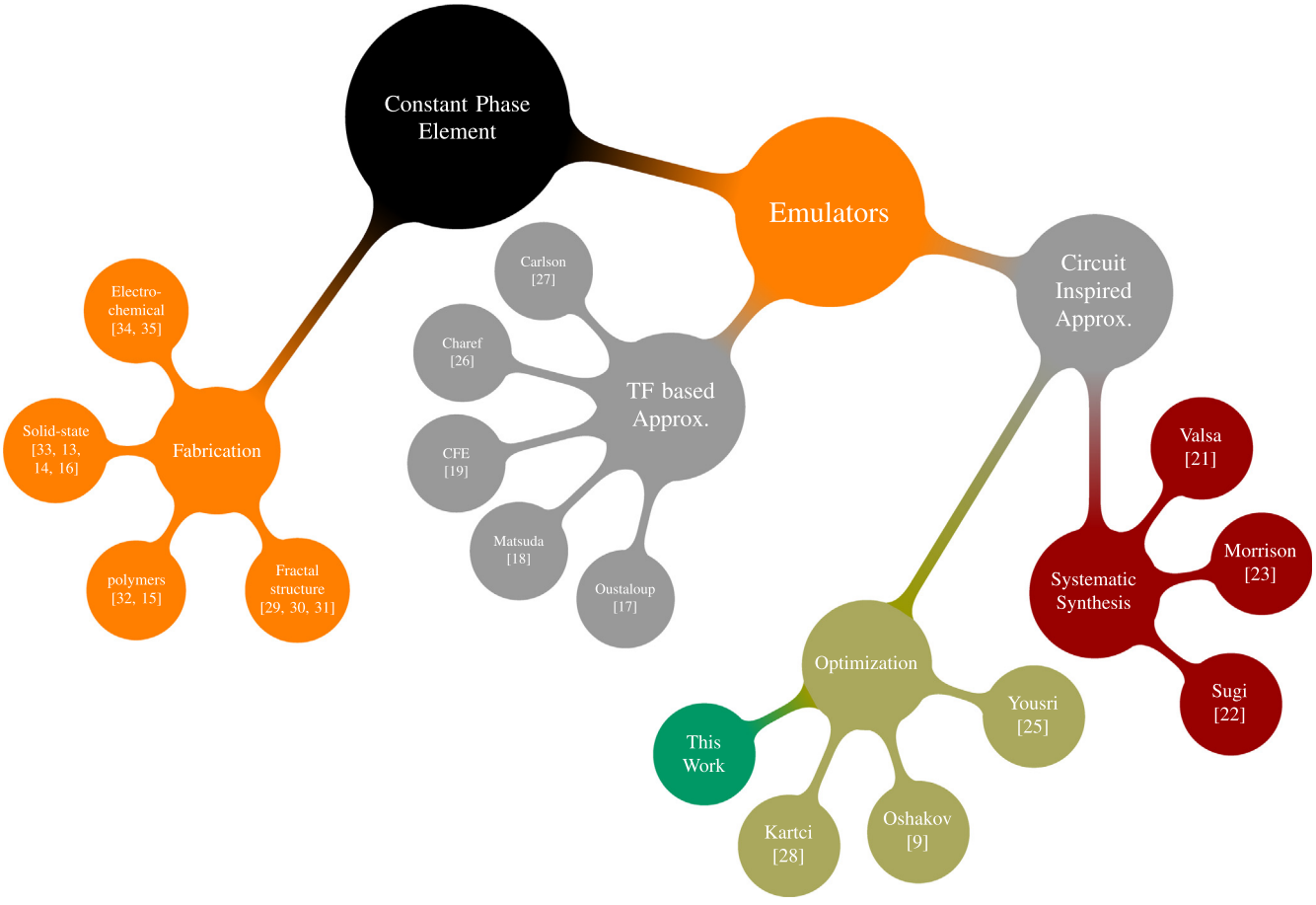

Fig. 1. Alternative approaches and different methods for approximating a CPE [9,13-19,21-23,25-35].

used [21–24]. In these passive realizations, optimization-based methods have recently been employed to calculate the optimum component values given a specific order of approximation and operating bandwidth [25,9].

This work contributes the following:

- a novel passive *RC* network structure based on crossbar arrays is used to approximate the CPE behavior.
- a meta-heuristic optimization algorithm is used to find the optimal parameters of the crossbar array in a 6-dimensional search space.
- The proposed CPE realization is compared against two other state-of-art realizations as a standalone and within the relaxation oscillator application.
- realization of multiple CPEs with different fractional orders while sharing the same load capacitance is demonstrated.

This paper is organized as follows: Section "Crossbar-based CPE approximation" introduces the crossbar realization of a CPE. The use of the flower pollination algorithm (FPA) to find the optimal parameter values is discussed in Section "Parameters identification". Sections "CPE design examples and comparison" and "Shared CPE design" illustrate different design examples including the single CPE and multiple CPEs sharing the same load.

Crossbar-based CPE approximation

Fig. 2(b) shows a general crossbar array with loading impedances and without parasitics for illustration. The programmable switching devices are represented as resistors. The crossbar array has m inputs and n outputs. To realize a grounded two-terminal CPE, one port only is needed and thus the other $m-1$ ports are grounded. The loading impedances, Z_{Ln}, should be capacitive in nature in order to realize a CPE. With all except one input grounded, the resistors within each row appear in parallel with the corresponding loads, as shown in Fig. 2(c). The equivalent admittance seen from the input terminal can be written as:

$$Y_{in}=\sum_{i=1}^{n}\frac{Z_{Li}+R_{Pi}}{Z_{Li}(R_{Pi}+R_{1i})+R_{Pi}R_{1i}}, \tag{2}$$

where Z_{Li} is the load impedance in the i^{th} column and R_{Pi} is the equivalent parallel resistance of the grounded inputs in the i^{th} column and its admittance equals $\sum_{j=1}^{m}1/R_{ji}$. In case of pure capacitive loading, the network has an equivalent input admittance of the form:

$$Y_{in}=\sum_{i=1}^{n}K_i\frac{1+s/\omega_{z_i}}{1+s/\omega_{p_i}}, \tag{3}$$

where $K_i=1/(R_{Pi}+R_{1i})$, $\omega_{z_i}=1/C_iR_{Pi}$, $\omega_{p_i}=1/(K_iC_iR_{Pi}R_{1i})=\omega_{z_i}/K_iR_{1i}$ and C_i is the capacitance of the i^{th} load.

In order to have a CPE response, the locations of zeros and poles of the previous equation should be alternating and should start with a zero. Also, this approximation can be seen as a weighted sum of low- and high-pass filters, which is a new implementation to the best of our knowledge. Some Previously proposed implementations were based on summations of either low- or high-pass filters [36,37].

It is worth noting that the well known parallel RC approximation is a special case of this approximation [37,38,25,36] where there are no grounded rows in the crossbar array. Mathematically, this can be obtained by setting $R_{Pi}=\infty$ yielding

$$Y_{in}=\sum_{i=1}^{n}\frac{sC_i}{1+sC_iR_{1i}}. \tag{4}$$

Parameters identification

Meta-heuristic optimization algorithms are used extensively nowadays to solve many science and engineering problems. This is due to the fact that traditional optimization algorithms (gradient-based) tend to converge to local optimal points and are sensitive to their initial search vector. However, in meta-heuristic algorithms, the stochastic movements of the search agents and

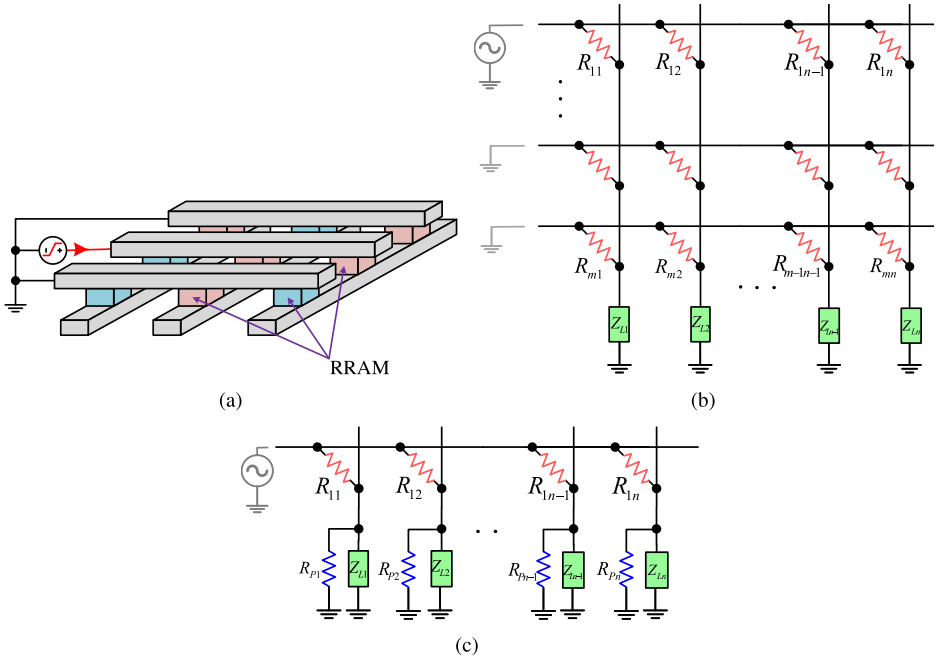

Fig. 2. (a) 3D crossbar array containing RRAMs (i.e., memristors), (b) resistive network of the crossbar array with general impedance loading, and (c) simplified model of the array for CPE approximation.

the random initial populations tend to overcome the drawbacks of gradient-based techniques [39]. These algorithms are more computationally exhaustive than gradient-based techniques, but they are less likely to fall into local solutions due to the explorations made to the entire search space. Researchers have been using meta-heuristics to tackle difficult design problems involving fractional-order systems [40,41]. For instance, one of the earliest contributions in this direction is the use of a differential evolution algorithm to design a fractional order filter with a certain magnitude response [42]. An IIR approximation of the digital fractional-order differentiators of orders $1/2, 1/3$, and $1/4$ were designed using flower pollination algorithm (FPA) and Moth Flame Optimizer (MFO) [43,44]. Also, many fractional-order analog filters approximating Butterworth, Chebyshev, and Bessel magnitude responses were designed with the help of Meta-heuristic optimization methods [45–51].

In this work, the utilized bio-inspired optimization algorithm is FPA, which is based on the pollination process in plants [39]. This algorithm has been recently used to extract the optimal transfer function parameters of the sum of high-pass filters in order to approximate the frequency behavior of the fractional-order Laplacian s^{α} [36]. A similar objective is sought in this work, which is to find the optimal circuit parameters that make the input admittance, from Eq. (2), $Y_{in} \approx C_{\alpha} s^{\alpha}$ where $\alpha \in [0, 1]$.

Instead of optimizing over $(m+1) \times n$ variables. The problem is simplified to search for the equivalent resistance of grounded branches, R_{Pi} which means that the search space is reduced to $3n$. Due to the nature of the problem which requires alternating poles and zeros with equal spacing to minimum ripple response (minimum phase error), it can be assumed that the ratio between every two successive poles or two successive zeros is fixed. Thus, we can further reduce the search space to 6 variables only; the first basic branch parameters and the next branches parameters are ratioed from the basic branch. Thus, the search vector is defined as $x = [R_{11}, R_{p1}, C_1, r_{R_1}, r_{R_p}, r_C]$, where R_{11}, R_{p1}, and C_1 are the first branch parameters (series resistor, parallel resistor, and load capacitor), r_{R_1}, r_{R_p}, and r_C are ratios that relate subsequent elements given as: $R_{1i} = R_{11}/r_{R_1}^{i-1}, R_{pi} = R_{p1}/r_{R_p}^{i-1}$ and $C_i = C_1/r_C^{i-1}$ where n = 2, ..., n.

The sum of the absolute relative magnitude and phase errors can be defined as:

$$f_{C_{\alpha}}(x) = \sum_{i=1}^{M} \left| \frac{\omega_i^{\alpha} C_{\alpha} - |Y_{in}(x, \omega_i)|}{\omega_i^{\alpha} C_{\alpha}} \right| \text{ and}$$

$$f_{\alpha}(x) = \sum_{i=1}^{M} \left| \frac{\alpha\pi/2 - \phi(Y_{in}(x, \omega_i))}{\alpha\pi/2} \right|, \tag{5}$$

respectively, where M is the number of frequency points. Hence, the optimization problem can formulated as minimizing the maximum error in phase and magnitude as follows:

$$\begin{aligned} \min_{x} \quad & \max(f_{\alpha}(x), f_{C_{\alpha}}(x)), \\ \text{s.t.} \quad & LL \leqslant x \leqslant UL \end{aligned} \tag{6}$$

where LL and UL are lower and upper limits.

In our simulations, we set the number of search agents to 42 and the maximum number of iterations to 3000. Half a decade on the left and half a decade on the right sides of the frequency range are also considered during the optimization to reduce errors near the ends of the frequency range under investigation.

CPE design examples and comparison

Let us consider the approximation of a CPE with $C_{\alpha} = 10\ \text{nF} \cdot \text{sec}^{\alpha-1}$ and with different phases in the frequency range $[10^6, 10^9]$ rad/s with 100 logarithmically-spaced frequency points per decade with $UL = [5M, 100M, 10n, 20, 20, 20]$ and $LL = [1, 0.1k, 1f, 1, 1, 1]$.

Table 1 summarizes the optimal values of the solution vector X obtained for $\alpha = 0.3, 0.5, 0.6$, and 0.8 using 54 independent runs. The consistency of FPA results are observed from the coefficient of variation (COV) values which are on average of order 10^{-3}. Fig. 3 (a) and (b) show the phase and the capacitance percentage errors over the frequency range $[10^6, 10^9]$ rad/s. It can be noticed that the phase error is not more than 5° for $\alpha = 0.8$, 3.5° for $\alpha = 0.5$ and 2° for $\alpha = 0.3$. The capacitance percentage error is not greater than 8.5% for $\alpha = 0.3$ and 7% for $\alpha = 0.5, 0.6$ and 0.3 respectively.

In order to compare the possible CPE realizations, we repeated the optimization algorithm for different numbers of branches and calculated the maximum relative error in the phase for different fractional orders. Fig. 3 ((e) and (f)) depicts this comparison with the aforementioned parameters which clearly shows that the interlaced approximation of (3) outperforms the parallel RC branch approximation (4) for the same number of branches with an error that is approximately the same regardless of the CPE order. If it is required to design a CPE with an error less than 1%, then the number of branches is 10 using (3) while it is 15 using (4) for a CPE order greater than 0.5.

Monte-Carlo simulations

Fig. 3(c) and (d) show the phase and pseudo-capacitance results of 200 Monte-Carlo simulations with 5% tolerance based on the optimal component values summarized in Table 1. The histograms are generated using 200×500 frequency points. The phase response shows an approximated normal distribution with mean and standard deviation values of $27.1 \pm 1.92^{\circ}, 45.2 \pm 2.2^{\circ}$, and $71.46 \pm 2.39^{\circ}$ for $\alpha = 0.3, 0.5$, and 0.8, respectively. Also, the pseudo-capacitance follows near normal distribution with mean and standard deviation values of $10.47 \pm 0.75\ \text{nF sec}^{\alpha-1}$, $10.04 \pm 0.78\ \text{nF sec}^{\alpha-1}$, and $10.18 \pm 1.12\ \text{nF sec}^{\alpha-1}$ at $\alpha = 0.3$, 0.5, and 0.8, respectively.

Comparison with other realizations

We selected two circuit inspired approximations from the mind map shown in Fig. 1 for comparison with the crossbar array tech-

Table 1
Optimal parameters values for selected fractional orders. The mean and coefficient of variation (COV) are summarized for 54 independent runs where $COV = std/mean$.

α	0.3		0.5		0.6		0.8	
	Mean	COV	Mean	COV	Mean	COV	Mean	COV
R_{11} (Ω)	2.71e6	4.27e − 3	1.22e5	4.16e − 3	3.11e4	1.56e − 3	3.49e3	6.31e − 3
R_{p1} (Ω)	9.93e7	5.97e − 3	8.19e7	8.85e − 2	7.96e7	1.06e − 1	7.61e7	1.62e − 1
C_1 (F)	5.22e − 13	4.21e − 3	7.44e − 12	4.16e − 3	2.84e − 11	2.14e − 3	2.84e − 10	2.28e − 3
r_{R1}	2.06	7.68e − 5	3.69	9.24e − 4	5.04	9.97e − 4	1.10e1	2.61e − 3
r_{R_p}	2.05	2.44e − 3	3.70	2.45e − 2	4.88	2.89e − 2	7.86	4.37e − 2
r_C	5.10	3.33e − 4	3.41	3.57e − 4	2.70	8.41e − 4	1.51	6.51e − 4
Fmin	1.27e1	6.97e − 6	1.05e1	7.92e − 6	9.35	3.22e − 5	8.64	9.67e − 5

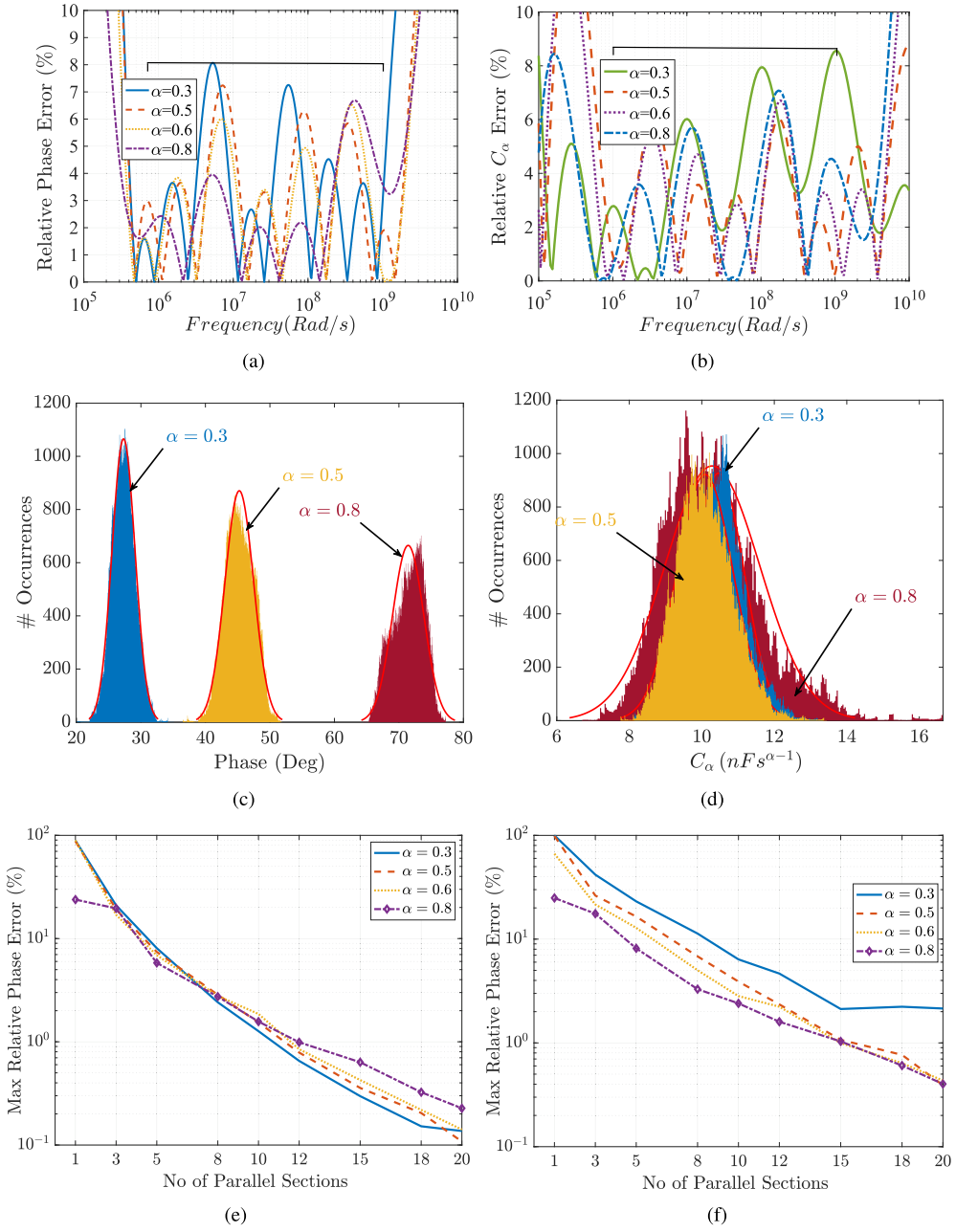

Fig. 3. (a) Phase error in degrees and (b) pseudo-capacitance percentage tolerance. (c) and (d) 200 Monte-Carlo simulations with 5% tolerance of phase and pseudo-capacitance, respectively. (e) and (f) Maximum relative phase error versus different number of branches for approximation using (3) and parallel RC approximation using (4), respectively.

nique. The chosen methods are the Valsa realization [21] and the optimization-based realization [25]. In the Valsa realization the designer can control the phase error, bandwidth or number of branches during the synthesis procedure. Table 3 shows the synthesized resistor and capacitor values of the Valsa network for different orders. On the other hand, the realization based on [25] is based on Sugi's approximation [22]. Thus it can be considered a special case of our proposed realization when R_p is set to ∞. The optimized resistor and capacitor values are shown in Table 4. The phase and pseudocapacitance errors are depicted in Table 2. Clearly, the proposed realization technique shows comparable results to Valsa's method and better results when compared to [25].

Application: fractional-order relaxation oscillator

In order to test the accuracy of the proposed crossbar realization, we used the designed circuits to realize a relaxation oscillator [52] shown in 4(a) where the CPE is implemented with both crossbar and Valsa realizations to compare the performance. In order to calculate the oscillation frequency numerically, we have simulated the circuit with MATLAB using the Grunwald-Letnikov (GL) based simulation technique as [53]:

$$V_{C_\alpha}(t_i) = \left(\frac{-V_{C_\alpha}(t_{i-1}) + V_{ch}}{R_b C_\alpha}\right) \times h^\alpha - \sum_{k=1}^{i} w_k^{(\alpha)} V_{C_\alpha}(t_{i-k}) \tag{7}$$

Table 2
Percentage capacitance and phase errors comparison between the proposed approach, Valsa [21], and sum of high-pass filters (Xbar w/o R_p) [25].

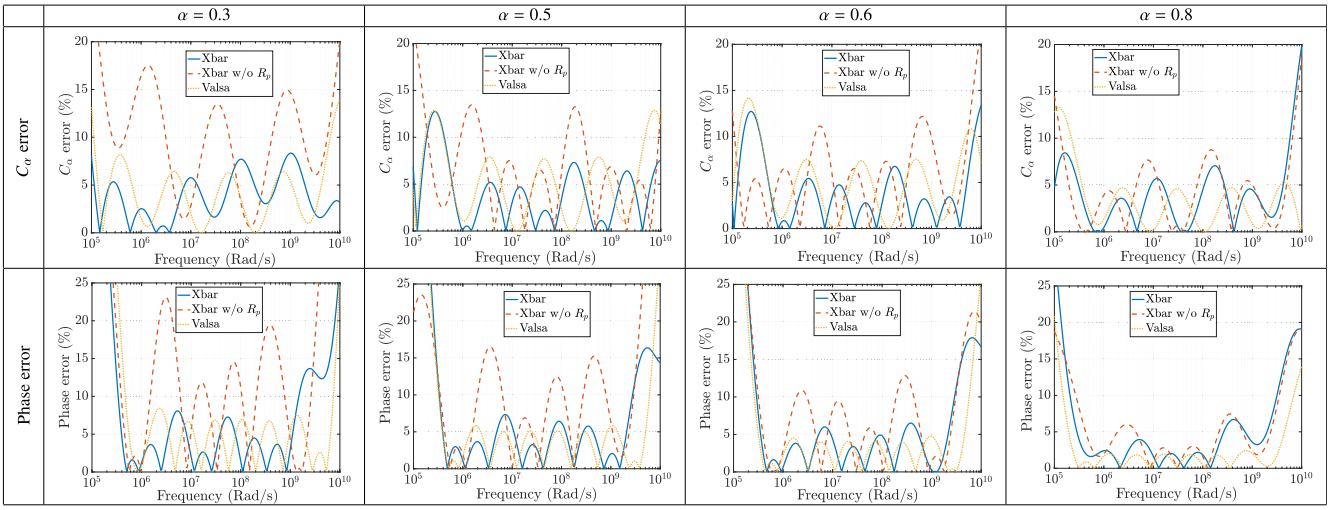

Table 3
Circuit parameters values generated using the Valsa algorithm where $i = 2, 3, 4$.

	$\alpha = 0.3$	$\alpha = 0.5$	$\alpha = 0.6$	$\alpha = 0.8$
$R_1(\Omega)$	2516495.38	129447.7	34123.7	3433.64
R_i/R_{i-1}	0.4687	0.2828	0.2197	0.1326
$C_1(nF)$	0.397	7.7	2.93	291.24
C_i/C_{i-1}	0.17	0.28	0.36	0.6
$R_p(\Omega)$	2852204.68	328219.04	121187.23	22465.35
$C_p(fF)$	0.4	68.9	810	9.7e4

Table 4
Optimal circuit parameters values for the proposed topology with no R_p.

	$\alpha = 0.3$	$\alpha = 0.5$	$\alpha = 0.6$	$\alpha = 0.8$
$R_{11}(\Omega)$	7593769.6	924747.6	49843.67	5060.02
$C_1(pF)$	12.7	65.3	65.8	364.58
r_{R1}	2.477	5.15	6.15	12.95
r_C	9.1	4.36	3.56	1.63

along with the switching condition: if $|V_{C_\alpha}(t_i)| = |\beta V_{ch}|$ then $V_{ch} = -V_{ch}$. Where $V_{C_\alpha}(t)$ is the voltage across CPE, V_{ch} is the charging/discharging voltage (either V_{cc} or $-V_{cc}$). The initial conditions used are $V_{C_\alpha}(0) = 0.1\beta V_{cc}, \beta = 0.5$ and $V_{ch} = V_{cc}$ where $V_{cc} = 5V$. The GL weights are calculated according to the recursive relation [53]:

$$w_0^{(\alpha)} = 1, \quad w_k^{(\alpha)} = \left(1 - \frac{\alpha+1}{k}\right) w_{k-1}^{(\alpha)} \tag{8}$$

The circuit simulations are run on Virtuoso using a CPE with the values reported in Tables 1 and 3 at $\alpha = 0.6$. R_a is set to 10 KΩ and R_b is swept to study the oscillation frequency against R_b to cover all the working range that we designed the CPE over as shown in Fig. 4(b). Clearly, both crossbar and Valsa approximations shows a comparable respsonse with less fluctuation in case of crossbar realization. The subplots in Fig. 4(b) show the transient simulations at $R_b = 5$ KHz giving 9.07 MHz and 7.95 MHz oscillation frequency with 16.5% and 2.16% percentage errors compared to ideal case for Valsa realization and crossbar realization, respectively.

Shared CPE design

In this section, we show that by only programming the crossbar array while fixing the load capacitances, different CPEs can be obtained.

Different CPEs sharing the capacitive loading

The first example here is to use the same hardware shown in Figure 2 and optimize over different resistances (R_s and R_p) for every CPE while sharing capacitor loading. Thus, we define the objective function to optimize over CPEs' phases as follows:

$$\begin{aligned} \min_x \quad & max(f_{\alpha 1}(x), \cdots, f_{\alpha k}(x)), \\ \text{s.t.} \quad & LL \leqslant x \leqslant UL \end{aligned} \tag{9}$$

where $\alpha_1, \ldots, \alpha_k$ are the desired fractional orders and the search vector is defined as $x = [R_{111}, R_{p11}, r_{R_1 1}, r_{R_p 1}, \cdots, R_{11k}, R_{p1k}, r_{R_1 k}, r_{R_p k}, C_1, r_C]$ to find the crossbar parameters with fixed loads for all fractional orders.

We conducted two experiments for a resistance-optimized CPE with $\alpha \in \{0.3, 0.4, 0.5\}$ and for a capacitance-optimized CPE with $\alpha \in \{0.6, 0.7, 0.8\}$. Fig. 5 shows the phase relative error result of the designed CPEs where the relative error increased to 6%, which is slightly higher than the fully optimized CPE in the previous section.

Multiple CPEs design

The crossbar array can be used as a multi port network to realize multiple CPEs at the same time. These CPEs would share the same load capacitances and grounded resistance branches as shown in Fig. 6(a). The objective function is defined by (9) except that R_p would be shared between the CPEs. Thus, the search vector is defined as $x = [R_{111}, r_{R_{11}}, \cdots, R_{11k}, r_{R_{1k}}, R_{p11}, r_{R_p 1}, C_1, r_C]$ where k is the number of CPE elements.

Fig. 6(b) and (c) show the results of the optimized devices for two sets of CPEs; the first realized set has fractional orders of 0.3, 0.4 and 0.5 and the second set has 0.6, 0.7 and 0.8 fractional orders at $n = 8$, respectively. The results show a relative phase error less than 5% and 7% for the two examples confirming the ability of this realization to share part of the circuit among the CPEs and still provide acceptable performance.

The value of the objective function versus the iteration number of four design examples are summarized in Table 5. The objective function is seen to be settled enough to consider the search convergent. In case of *CPE* with R_p (Section "CPE design examples and comparison"), the final value of the objective functions are reached before iteration number 1500 except the case of $\alpha = 0.8$ where it settles about iteration number 1700. The final objective function

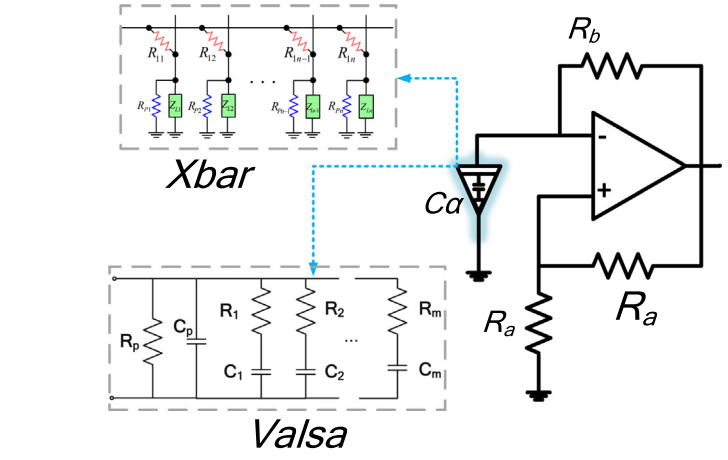

(a)

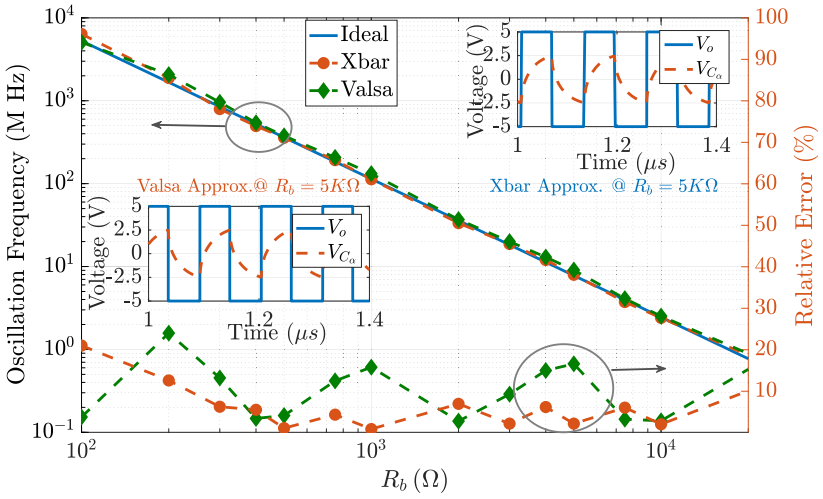

(b)

Fig. 4. (a) Fractional-order relaxation oscillator circuit schematic and (b) obtained oscillation on the left y-axis and relative error percentage on right y-axis with changing R_b. Subplots show the transient simulation of the output voltage V_o and the CPE voltage V_{C_α}.

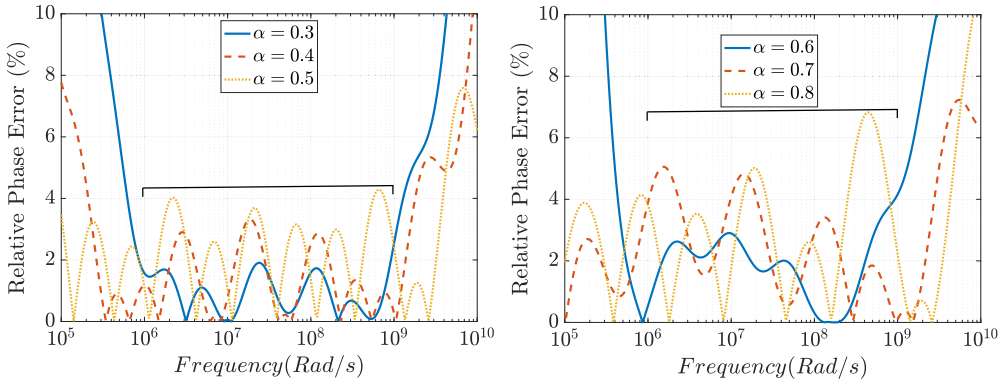

(a) (b)

Fig. 5. (a) Phase relative error for different fractional-orders with same capacitive loading with $n = 8$.

values decrease by increasing α. A similar behaviour is seen for the case of *CPE* with $R_p = \infty$ (Section "Comparison with other realizations"). However, the final values of the objective function are larger than the previous case which is in accordance with the discussion of Fig. 3 (e,f). The final case is the multiple CPE design. It shows discrepancy in convergence speed between its two studied examples. The first example at $\alpha = 0.6, 0.7$, and 0.8 has the slowest convergence rate near iteration number 6500 while the other case at $\alpha = 0.3, 0.4$, and 0.5 has converged near iteration number 4000.

Table 5
Convergence curves for 3 investigated designs.

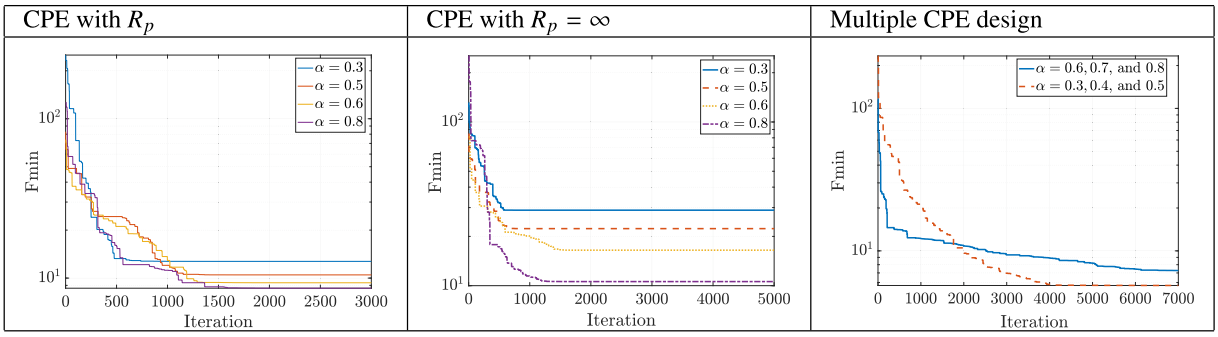

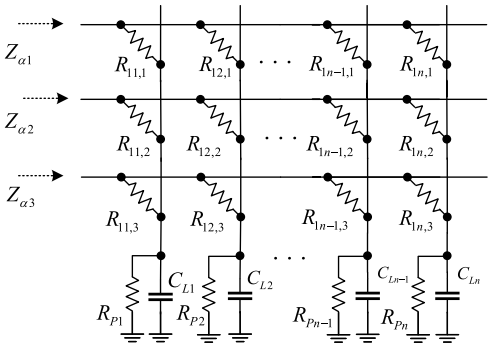

(a)

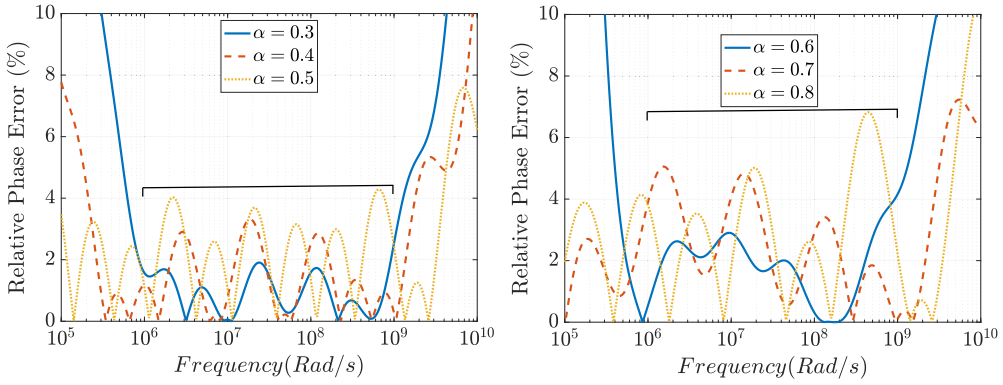

(b) (c)

Fig. 6. (a) Equivalent circuit schematic of separate multiple CPEs design. (b) and (c) Relative phase error for different fractional-orders sharing the same capacitive loading with $n = 8$.

Conclusion and future work

In this work, a new realization of the CPE using crossbar arrays was introduced. The optimal circuit component values were obtained using a minimax objective function and a meta-heuristic optimization algorithm. Compared to the parallel *RC* branches approach, the proposed method showed less error in phase and magnitude responses for the same number of branches *n*. The effect of varying *n* on the error performance and sensitivity analysis of component tolerances using Monte-Carlo simulations were discussed. The introduced topology can simultaneously realize multiple CPEs sharing the same circuits to save the area. The main limitation of our work is that the programmable resistive device must have a wide range. Using the proposed approximation in applications such as fractional-order filters and oscillators will be considered in our future work with experiments.

Compliance with Ethics Requirements

This article does not contain any studies with human or animal subjects.

Declaration of Competing Interest

The authors declare that they have no known competing financial interests or personal relationships that could have appeared to influence the work reported in this paper.

References

[1] Xia Q, Yang JJ. Memristive crossbar arrays for brain-inspired computing. Nat Mater 2019;18:309–23.
[2] Pi S, Li C, Jiang H, Xia W, Xin H, Yang JJ, Xia Q. Memristor crossbar arrays with 6-nm half-pitch and 2-nm critical dimension. Nat Nanotechnol 2019;14:35–9.
[3] Yu M, Cai Y, Wang Z, Fang Y, Liu Y, Yu Z, et al. Novel vertical 3d structure of tao x-based rram with self-localized switching region by sidewall electrode oxidation. Sci Rep 2016;6:21020.
[4] Sebastian A, Le Gallo M, Khaddam-Aljameh R, Eleftheriou E. Memory devices and applications for in-memory computing. Nat Nanotechnol 2020:1–16.
[5] Fouda M, Kurdahi F, Eltawil A, Neftci E. Spiking neural networks for inference and learning: A memristor-based design perspective. arXiv preprint arXiv:1909.01771; 2019.
[6] Mahmoodi MR, Nili H, Strukov DB. Rx-puf: Low power, dense, reliable, and resilient physically unclonable functions based on analog passive rram crossbar arrays. In: 2018 IEEE symposium on VLSI technology. IEEE; 2018. p. 99–100.
[7] Fouda ME, Eltawil AM, Kurdahi F. Modeling and analysis of passive switching crossbar arrays. IEEE Trans Circ Syst I Regul Pap 2018;65:270–82.
[8] Elwakil AS. Fractional-order circuits and systems: An emerging interdisciplinary research area. IEEE Circ Syst Mag 2010;10:40–50.
[9] Ushakov PA, Maksimov KO, Stoychev S, Gravshin V, Kubanek D, Koton J. Synthesis of elements with fractional-order impedance based on homogenous distributed resistive-capacitive structures and genetic algorithm. J Adv Res 2020:25:275–283.
[10] Valério D, Da Costa JS. Introduction to single-input, single-output fractional control. IET Control Theory Appl 2011;5:1033–57.
[11] Shah ZM, Kathjoo MY, Khanday FA, Biswas K, Psychalinos C. A survey of single and multi-component fractional-order elements (foes) and their applications. Microelectron J 2019;84:9–25.
[12] Buscarino A, Caponetto R, Graziani S, Murgano E. Realization of fractional order circuits by a constant phase element. Eur J Control 2020;54:64–72.
[13] John DA, Banerjee S, Bohannan GW, Biswas K. Solid-state fractional capacitor using mwcnt-epoxy nanocomposite. Appl Phys Lett 2017;110:163504.
[14] Adhikary A, Khanra M, Sen S, Biswas K. Realization of a carbon nanotube based electrochemical fractor. In: 2015 IEEE international symposium on circuits and systems (ISCAS). IEEE; 2015. p. 2329–32.
[15] Agambayev A, Farhat M, Patole SP, Hassan AH, Bagci H, Salama KN. An ultra-broadband single-component fractional-order capacitor using mos2-ferroelectric polymer composite. Appl Phys Lett 2018;113:093505.
[16] Elshurafa AM, Almadhoun MN, Salama K, Alshareef H. Microscale electrostatic fractional capacitors using reduced graphene oxide percolated polymer composites. Appl Phys Lett 2013;102:232901.
[17] Oustaloup A, Moreau X, Nouillant M. The crone suspension. Control Eng Pract 1996;4:1101–8.
[18] Khoichi M, Hironori F. h_∞optimized waveabsorbing control: Analytical and experimental result. J Guid Control Dyn 1993;16:1146–53.
[19] Roy S. On the realization of a constant-argument immittance or fractional operator. IEEE Trans Circ Theory 1967;14:264–74.
[20] Tsirimokou G, Kartci A, Koton J, Herencsar N, Psychalinos C. Comparative study of discrete component realizations of fractional-order capacitor and inductor active emulators. J Circ Syst Comput 2018;27:1850170.
[21] Valsa J, Dvorak P, Friedl M. Network model of the cpe. Radioengineering 2011;20:619–26.
[22] Sugi M, Hirano Y, Miura Y, Saito K. Frequency behavior of self-similar ladder circuits. Colloids Surf A 2002;198:683–8.
[23] Morrison R. Rc constant-argument driving-point admittances. IRE Trans Circ Theory 1959;6:310–7.
[24] Fouda ME, AboBakr A, Elwakil AS, Radwan AG, Eltawil AM. Simple mos transistor-based realization of fractional-order capacitors. In: 2019 IEEE international symposium on circuits and systems (ISCAS). IEEE; 2019. p. 1–4.
[25] Yousri D, AbdelAty AM, Radwan AG, Elwakil A, Psychalinos C. Comprehensive comparison based on meta-heuristic algorithms for approximation of the fractional-order Laplacian s^{α} as a weighted sum of first-order high-pass filters. Microelectron J 2019;87:110–20.
[26] Charef A, Sun H, Tsao Y, Onaral B. Fractal system as represented by singularity function. IEEE Trans Automatic Control 1992;37:1465–70.
[27] Carlson GE, Halijak C. Simulation of the fractional derivative operator and the fractional integral operator Ph.D. thesis. Kansas State University; 1960.
[28] Kartci A, Agambayev A, Farhat M, Herencsar N, Brancik L, Bagci H, et al. Synthesis and optimization of fractional-order elements using a genetic algorithm. IEEE Access 2019;7:80233–46.
[29] Jesus IS, Machado JT. Development of fractional order capacitors based on electrolyte processes. Nonlinear Dyn 2009;56:45–55.
[30] Haba TC, Ablart G, Camps T. The frequency response of a fractal photolithographic structure. IEEE Trans Dielectr Electr Insul 1997;4:321–6.
[31] Haba TC, Ablart G, Camps T, Olivie F. Influence of the electrical parameters on the input impedance of a fractal structure realised on silicon. Chaos Solitons Fract 2005;24:479–90.
[32] Caponetto R, Graziani S, Pappalardo FL, Sapuppo F. Experimental characterization of ionic polymer metal composite as a novel fractional order element. Adv Math Phys 2013;2013.
[33] Buscarino A, Caponetto R, Di Pasquale G, Fortuna L, Graziani S, Pollicino A. Carbon black based capacitive fractional order element towards a new electronic device. AEU Int J Electron Commun 2018;84:307–12.
[34] Biswas K, Sen S, Dutta PK. Realization of a constant phase element and its performance study in a differentiator circuit. IEEE Trans Circ Syst II Express Briefs 2006;53:802–6.
[35] Mondal D, Biswas K. Packaging of single-component fractional order element. IEEE Trans Device Mater Reliab 2013;13:73–80.
[36] AbdelAty AM, Elwakil AS, Radwan AG, Psychalinos C, Maundy BJ. Approximation of the fractional-order Laplacians$^{\alpha}$ as a weighted sum of first-order high-pass filters. IEEE Trans Circ Syst II Express Briefs 2018;65:1114–8.
[37] Sugi M, Hirano Y, Miura YF, Saito K. Simulation of fractal immittance by analog circuits: an approach to the optimized circuits. IEICE Trans Fundam Electron Commun Comput Sci 1999;82:1627–35.
[38] Gonzalez E, Dorčák Ľ, Monje C, Valsa J, Caluyo F, Petráš I. Conceptual design of a selectable fractional-order differentiator for industrial applications. Fract Calculus Appl Anal 2014;17.
[39] Yang X-S. Flower pollination algorithm for global optimization. In: Durand-Lose J, Jonoska N, editors. Unconventional computation and natural computation. Berlin, Heidelberg: Springer; 2012. p. 240–9.
[40] Gholami-Boroujeny S, Bolic M. Extraction of cole parameters from the electrical bioimpedance spectrum using stochastic optimization algorithms. Med Biol Eng Comput 2016;54:643–51.
[41] Yang Y, Ni W, Sun Q, Wen H, Teng Z. Improved cole parameter extraction based on the least absolute deviation method. Physiol Meas 2013;34:1239.
[42] Matos C, Ortigueira MD. Fractional filters: an optimization approach. In: Doctoral conference on computing, electrical and industrial systems. Springer. p. 361–6.
[43] Mahata S, Saha SK, Kar R, Mandal D. Optimal design of fractional-order digital differentiator using flower pollination algorithm. J Circ Syst Comput 2018;27:1850129.
[44] Mahata S, Saha SK, Kar R, Mandal D. A metaheuristic optimization approach to discretize the fractional order laplacian operator without employing a discretization operator. Swarm Evolution Comput 2019;44:534–45.
[45] Mahata S, Kar R, Mandal D. Optimal fractional-order highpass butterworth magnitude characteristics realization using current-mode filter. AEU Int J Electron Commun 2019;102:78–89.
[46] Mahata S, Banerjee S, Kar R, Mandal D. Revisiting the use of squared magnitude function for the optimal approximation of (1+α)-order butterworth filter. AEU Int J Electron Commun 2019;110:152826.
[47] Mahata S, Kar R, Mandal D. Comparative study of nature-inspired algorithms to design (1+α) and (2+α)-order filters using a frequency-domain approach. Swarm Evolution Comput 2020;55:100685.
[48] Mahata S, Kar R, Mandal D. Optimal rational approximation of bandpass butterworth filter with symmetric fractional-order roll-off. AEU Int J Electron Commun 2020;117:153106.
[49] Soni A, Sreejeth N, Saxena V, Gupta M. Series optimized fractional order low pass butterworth filter. Arab J Sci Eng 2020;45:1733–47.
[50] Soni A, Gupta M. Analysis and design of optimized fractional order low pass bessel filter. J Circ Syst Comput. https://doi.org/10.1142/S0218126621500353.
[51] Soni A, Gupta M. Performance evaluation of different order fractional chebyshev filter using optimisation techniques. Int J Electron Lett 2020;8:205–22.
[52] Radwan AG, Maundy BJ, Elwakil AS. Fractional-order oscillators. Oscillator Circ Front Des Anal Appl 2016;32:25.
[53] Petráš I. Fractional-Order Nonlinear Systems. Berlin Heidelberg: Springer; 2011.